Molecular Vision 2026; 32:325-341 <http://www.molvis.org/molvis/v32/325>
Received 11 June 2025 | Accepted 20 July 2026 | Published 5 August 2026

© 2026 Molecular Vision

Tasquinimod reduces retinal ischemia and pathological angiogenesis in an oxygen-induced retinopathy model

Fangfang Ji, Ji Zhang, Ji Jin

Department of Ophthalmology, the Second Affiliated Hospital of Soochow University, Jiangsu Province, China

Purpose: Ischemic retinal diseases, such as retinopathy of prematurity, retinal vein occlusion, and diabetic retinopathy, are leading causes of vision loss. Current treatments focus on late-stage complications and have significant limitations. S100A9, a calcium-binding protein involved in inflammation and angiogenesis, remains understudied in ischemic retinal diseases. This study aimed to investigate S100A9 expression in oxygen-induced retinopathy (OIR) mice and assess the therapeutic effects of the S100A9 inhibitor tasquinimod.

Methods: OIR was induced in C57BL/6J mice, and tasquinimod (10 mg/kg/d) was administered orally from P12 to P17. Retinal nonperfusion areas were analyzed using immunofluorescence, and angiogenesis-related markers were examined by reverse transcription quantitative polymerase chain reaction (RT-qPCR) and western blotting. Human retinal microvascular endothelial cells (HRECs) were exposed to cobalt chloride–induced hypoxia, treated with tasquinimod, and assessed for S100A9 and angiogenesis-related marker expression, as well as migration and tube formation.

Results: Tasquinimod significantly reduced retinal nonperfusion areas in OIR mice. RT-qPCR and western blot analysis showed that tasquinimod suppressed S100A9, VEGF, ICAM-1, and TSP-1 expression. In vitro, hypoxia upregulated S100A9 and HIF-1α in HRECs, while tasquinimod dose-dependently inhibited hypoxia-induced migration, tube formation, and the expression of angiogenesis-related factors, including HIF-1α, VEGF, ICAM-1, and TSP-1.

Conclusions: S100A9 is upregulated in ischemic retinal conditions and promotes pathological angiogenesis. Tasquinimod effectively inhibits retinal neovascularization by targeting S100A9 and downstream angiogenic pathways, highlighting its potential as a therapeutic strategy for ischemic retinal diseases.

Ischemic retinal diseases, such as diabetic retinopathy (DR), retinal vein occlusion (RVO), and retinopathy of prematurity (ROP), represent major causes of irreversible visual impairment across different age groups [1,2]. DR, in particular, is the leading cause of blindness among the working-age population, affecting approximately one-third of individuals with diabetes worldwide [3]. By 2030, the global diabetic population is projected to exceed 550 million, with DR cases surpassing 220 million [4]. RVO is the second most prevalent retinal vascular disorder, with an estimated global prevalence of 0.77%, impacting over 28 million individuals aged 30 to 89 years [5]. In neonates, ROP remains a leading cause of childhood blindness, particularly in low- and middle-income countries, where neonatal survival rates are rising but access to timely screening and treatment remains limited [1]. According to a global burden of disease analysis, ROP accounted for approximately 101,600 cases of vision impairment in 2019, including moderate and severe visual loss as well as blindness. The incidence of new-onset ROP is notably higher in regions such as Africa and East Asia, and without early intervention, its burden is projected to grow [6].

Correspondence to: Ji Jin, Department of Ophthalmology, the Second Affiliated Hospital of Soochow University, Suzhou 215004, Jiangsu Province, China; Phone: 0512-67783408; email: Jinji1055@suda.edu.cn

The retina is one of the most metabolically active tissues in the human body. Under ischemic conditions, the imbalance between oxygen demand and supply leads to neovascular complications that underlie vision-threatening stages of these diseases [7]. Currently available treatments, including laser photocoagulation, intravitreal anti–vascular endothelial growth factor (VEGF) injections, and vitrectomy, primarily target late-stage complications. While these interventions mitigate disease progression, they often entail retinal damage, require repeated administrations, or are limited by transient efficacy and cost [8-10]. Notably, anti-VEGF therapy has shown significant clinical efficacy but is limited by transient effects, the need for repeated injections, financial burden, and potential retinal atrophy due to vascular and neuronal degeneration [11,12]. Therefore, identifying upstream regulators of ischemia-induced angiogenesis is critical for developing more effective therapeutic strategies.

The oxygen-induced retinopathy (OIR) mouse model is a well-established platform for studying hypoxia-driven retinal neovascularization [13]. While OIR does not fully mimic the metabolic disturbances seen in DR, it shares crucial characteristics with various ischemic retinal diseases, including early vascular loss, aberrant neovascularization, breakdown of the blood–retinal barrier, plasma leakage, and neuroinflammatory responses [14]. Hence, it provides a practical in

vivo system for investigating angiogenic mechanisms and evaluating potential therapeutic interventions.

Emerging evidence implicates the damage-associated molecular pattern (DAMP) protein S100A9 as a mediator of inflammation and vascular pathology [15]. S100A9 is abundantly expressed in myeloid cells and acts via pattern recognition receptors such as Toll-like receptor 4 (TLR4) and the receptor for advanced glycation end products (RAGE) [15-18], triggering downstream MAPK, PI3K, and NF-κB pathways to upregulate proinflammatory and angiogenic mediators including IL-6, CCL2, ICAM-1, and VCAM-1 [19-25]. SERPINE1 has also been implicated in S100A9-induced suppression in MDS [26]. These inflammatory responses contribute to vascular permeability [27], endothelial proliferation, migration, and pathological neovascularization [28]. Moreover, S100A9 has been associated with multiple inflammatory diseases, including arthritis [29], inflammatory bowel disease [30], and diabetes [31].

Members of the S100 protein family have been implicated in ocular neovascularization, particularly under ischemic and inflammatory conditions [32-34]. For example, S100A4 has been reported to promote neovascularization in the OIR model [32,33]. However, the role of S100A9 in ischemic retinal angiogenesis remains uncharacterized. This is particularly relevant given recent proteomic analyses identifying S100A9 upregulation in OIR mice and in the vitreous of patients with proliferative diabetic retinopathy [21,35].

Tasquinimod is a small-molecule oral inhibitor with high affinity for S100A9, preventing its interaction with TLR4 and RAGE [36]. It has demonstrated antiangiogenic activity in prostate cancer models and is currently under clinical evaluation for multiple myeloma (NCT04405167) [37,38]. Mechanistically, tasquinimod modulates the expression of thrombospondin 1 (TSP-1) and suppresses hypoxia-inducible factor 1α (HIF-1α) signaling [39-41], implicating these pathways in its antiangiogenic effects. However, its potential to attenuate ischemia-induced retinal neovascularization has not been investigated.

This study aims to evaluate the expression changes of S100A9 in the OIR mouse model and to investigate the therapeutic potential of tasquinimod in attenuating retinal neovascularization. In addition, we examined the effects of tasquinimod on human retinal capillary endothelial cells (HRECs) under hypoxic conditions, which serve as an in vitro model to mimic the ischemic microenvironment of the retina. Using this approach, we assessed the inhibitory effects of tasquinimod on hypoxia-induced endothelial migration and vascular network formation. By characterizing the expression dynamics of S100A9 and the antiangiogenic responses to tasquinimod, this study provides mechanistic insights and supports the therapeutic potential of S100A9 inhibition in ischemia-associated retinal vascular pathology.

METHODS

Ethical approval: All animal experiments were conducted in compliance with the Guidelines for the Care and Use of Laboratory Animals of the Chinese Medical Academy and adhered to the Association for Research in Vision and Ophthalmology (ARVO) Statement for the Use of Animals in Ophthalmic and Vision Research. The study was approved by the Animal Care Committee of Soochow University, Suzhou, China, and all experimental procedures followed the regulations set forth by the Laboratory Animal Management Committee of Soochow University.

OIR mouse model: C57BL/6J mice were obtained from Shanghai SLAC Laboratory Animal Co. Ltd. (Shanghai, China) and housed under specific pathogen-free conditions with a 12-h light–dark cycle, receiving a standard laboratory diet and water ad libitum. OIR was induced as previously described [42]. Briefly, postnatal (P) day 7 mouse pups were exposed to 75% oxygen (hyperoxia) in a sealed chamber until P12, then returned to room air (21% oxygen; normoxia) until P17. Mice were randomly assigned to five experimental groups: (1) normal group (n = 7): mice maintained under normoxia throughout the experiment; (2) OIR12 group (n = 14): mice exposed to 75% oxygen from P7 to P12; (3) OIR17 group (n = 14): mice exposed to 75% oxygen from P7 to P12, followed by normoxia until P17; (4) OIR12 + Tas 5d group (n = 14): mice exposed to 75% oxygen from P7 to P12, followed by oral administration of tasquinimod (10 mg/kg/d) from P12 to P17 under normoxia; and (5) OIR12 + PBS 5d group (n = 14): mice exposed to 75% oxygen from P7 to P12, followed by oral administration of phosphate-buffered saline (PBS) (10 mg/kg/d) from P12 to P17 under normoxia. Although formal power analysis was not conducted, group sizes were selected based on prior studies using the OIR model that detect treatment-related differences in retinal nonperfusion areas [13].

Tasquinimod preparation and administration: For in vitro use, tasquinimod (Absin Bioscience, Shanghai, China) was dissolved in 100% DMSO to prepare a concentrated stock of 10 mM. Working solutions for cell-based assays were freshly prepared by diluting the stock into culture medium to 1 to 5 μM; the final DMSO content was ≤0.05% v/v at 5 μM. Vehicle controls were DMSO-matched to the highest DMSO percentage used in the corresponding experiment.

For in vivo use, tasquinimod powder was dissolved in DMSO to a concentrated stock of 100 mg/ml, then diluted

with PBS to a 1-mg/ml working solution (final DMSO ≤1% v/v). Neonatal mice received 10 mg/kg once daily by oral administration (gavage) at 10 ml/kg from P12 to P17. To minimize systemic toxicity in neonatal mice, PBS was used as the vehicle control instead of DMSO alone; although pharmacologic matching was not achieved, ethical considerations informed this decision.

Retina isolation, isolectin staining, and retinal vasculature analysis: To visualize the retinal vasculature, retinal dissection and vessel staining were performed as described by Tual-Chalot et al. [43]. Postnatal mice were sacrificed by cervical dislocation, and the eyeballs were carefully enucleated. The eyes were fixed in 4% paraformaldehyde at room temperature for 10 to 15 min. After fixation, the cornea, sclera, uveal tissue, and lens were removed, and the isolated retinas were washed in PBS. For reverse transcription quantitative polymerase chain reaction (RT-qPCR) analysis, retinas were immediately transferred to RNA Later and stored at −80 °C.

For whole-mount immunostaining, the retinas were flattened by making four radial cuts and further fixed in −20 °C methanol to enhance permeabilization. Retinas were incubated overnight at 4 °C with isolectin-B4, an endothelial cell-specific marker, followed by 4′,6-diamidino-2-phenylindole nuclear staining. Immunofluorescence images were acquired using a Nikon (Tokyo, Japan) OFN25 fluorescence microscope (4× magnification).

Quantification of retinal nonperfusion area: The nonperfusion area of the retina was measured according to the method described by Smith et al. [44]. Images of the entire retina were stitched together using Photoshop CS6 (Adobe, San Jose, CA), and the lasso tool was used to outline the avascular regions and the total retinal area. The ratio of avascular area to total retinal area (in pixels) was calculated to determine the relative size of the nonperfusion zone. To minimize subjective bias, the analysis was performed by an independent investigator blind to the experimental groups. For each group, measurements were obtained from three retinas, with each retina analyzed three times, and the average value was used. Representative images are included in this study.

Retinal tissue protein extraction and purification: Retinal tissues were rapidly frozen in liquid nitrogen and ground into a fine powder using a mortar and pestle. The powdered tissue was transferred to a 5-ml centrifuge tube, and four volumes of lysis buffer (8 M urea, 1% protease inhibitor cocktail; Calbiochem, Merck, Darmstad, Germany) were added. The mixture was sonicated three times on ice using a high-intensity ultrasonic processor (Ningbo Scientz Biotechnology Co., Ltd., Zhejiang, China) to ensure complete lysis. The homogenate was centrifuged at 12,000g at 4 °C for 10 min, and the supernatant containing retinal protein extract was collected. The protein concentration of each sample was determined using the bicinchoninic acid (BCA) protein assay kit (Beyotime, Jiangsu, China).

Cell culture: HRECs were obtained from the BeNa Culture Collection (BNCC340909, Beijing, China) and cultured in Dulbecco's modified Eagle's medium (DMEM) supplemented with 10% fetal bovine serum. Cells were maintained at 37 °C in a humidified incubator with 5% CO_2. Cell morphology and growth were monitored daily under an inverted microscope, and the culture medium was refreshed every 2 to 3 days. When cells reached approximately 80% confluence, cells were subcultured immediately (within ≤2 h of assessment) at a 1:2 ratio; cultures were not maintained beyond confluence.

Hypoxia induction in HRECs: For hypoxia modeling, 200 µM cobalt chloride ($CoCl_2$) was applied for 24 h to chemically stabilize HIF-1α, thereby mimicking the ischemic microenvironment [45-47]. Cells were divided into the following groups for analysis: (1) control (normoxia), (2) hypoxia ($CoCl_2$ 200 µM, 24 h), (3) hypoxia + 1 µM tasquinimod (cotreatment with $CoCl_2$ for 24 h), and (4) hypoxia + 5 µM tasquinimod (cotreatment with $CoCl_2$ for 24 h).

Cell migration assay: Cell migration was assessed using the Transwell migration assay as described previously [39]. HRECs in the logarithmic phase were suspended in serum-free DMEM and adjusted to a concentration of 1×10^5 cells/ml. A 24-well Transwell system was used, with 600 µl of medium containing 200 µM $CoCl_2$ and different tasquinimod concentrations added to the lower chamber. A total of 150 µl of the cell suspension was seeded into the upper chamber and incubated at 37 °C with 5% CO_2 for 24 h. After incubation, the Transwell inserts were carefully removed, and the nonmigrated cells were wiped off. Migrated cells on the lower membrane surface were fixed with methanol for 30 min at room temperature and stained with crystal violet solution (15–30 min at room temperature). The membranes were washed with PBS, air-dried, and visualized under a 200× microscope, and the number of migrated cells was counted.

Tube formation assay: A Matrigel-based tube formation assay was performed to evaluate the angiogenic potential of HRECs as described previously [40]. Matrigel, µ-Slide angiogenesis slides, and 200-µl pipette tips were precooled at 4 °C for 20 min. A 10-µl aliquot of Matrigel was pipetted into each well, ensuring the absence of air bubbles, and incubated at 4 °C for 30 min, followed by polymerization at 37 °C for 30 to 60 min. HRECs were trypsinized (0.25% trypsin, 1–2 min), neutralized with complete medium, centrifuged at 200 ×g for 5 min, and resuspended at a density of 4×10^4 cells/well. Medium containing 200 µM $CoCl_2$ with or without tasquinimod was

Table 1. Primer sequences of human genes using in the real-time PCR.

Human Gene	Primer	Sequence (5′ to 3′)	Tm (°C)	Product (bp)
β-actin	Forward	GTCACCAACTGGGACGACAT	59.97	181
	Reverse	TAGCAACGTACATGGCTGGG	60.11	
HIF-1α	Forward	CCCAATGTCGGAGTTTGGAA	58.1	144
	Reverse	TGGCTGCATCTCGAGACTTT	59.39	
TSP-1	Forward	AGTCGTCTCTGCAACAACCC	60.25	120
	Reverse	GGGATTGGACAGGCATCCAT	59.81	
VEGF	Forward	CTTGCCTTGCTGCTCTACCT	60.04	123
	Reverse	GCAGTAGCTGCGCTGATAGA	59.97	
ICAM-1	Forward	AGGATGGCACTTTCCCACTG	59.96	131
	Reverse	GGAGAGCACATTCACGGTCA	60.04	
S100A9	Forward	GGTCATAGAACACATCATGGAGG	58.62	155
	Reverse	GGCCTGGCTTATGGTGGTG	60.75	

added, and the cells were incubated at 37 °C. Tube formation was captured after 8 h, and representative images were recorded for analysis.

RNA extraction and real-time RT-qPCR: Total RNA was extracted from mice retinal tissues or HREC samples using TRIzol reagent (Thermo Fisher Scientific, Waltham, MA) following the manufacturer's instructions. RNA was reverse-transcribed into complementary DNA (cDNA) using the PrimeScript RT Reagent Kit (Takara, Tokyo, Japan). RT-qPCR was performed with the SYBR Green PCR Kit (Takara) on a LightCycler 96 System (Roche Diagnostics, Mannheim, Germany). β-Actin was used as an internal control for normalization. Primer sequences for TSP-1, HIF-1α, VEGF, ICAM-1, and S100A9 were synthesized by GenScript (Nanjing, China), with the sequences described in Table 1 (human gene) and Table 2 (mouse gene).

Protein extraction and western blotting: HRECs were lysed in protein lysis buffer (50 mM Tris-HCl, pH 7.5, 2% sodium dodecyl sulfate, and 1 mM phenylmethylsulfonyl fluoride [PMSF]), with PMSF freshly added to 1 mM before use. Protein concentration was determined using the BCA Protein Assay Kit (Beyotime, Shanghai, China). Proteins were separated by sodium dodecyl sulfate–polyacrylamide gel electrophoresis, transferred to nitrocellulose membranes (MilliporeSigma, Burlington, MA), and blocked with 5% skimmed milk in PBS-T (PBS + Tween-20) at room temperature for 1 h. The membranes were incubated overnight at 4 °C with primary antibodies against HIF-1α, S100A9, TSP-1, VEGF, ICAM-1, and β-actin (catalog no. ab179483, EPR3555, ab267388, A4782, A12303, ab53013, and AC038; Abcam, Cambridge, UK). Horseradish peroxidase–conjugated secondary antibodies (A0208; Beyotime) were applied for 1 h at room temperature. Proteins were visualized using enhanced chemiluminescence (ECL; Millipore), and band intensities were quantified using ImageJ software (National

Table 2. Primer sequences of mouse genes using in the real-time PCR.

Mouse Gene	Primer	Sequence (5′ to 3′)	Tm (°C)	Product (bp)
β-actin	Forward	GGCTGTATTCCCCTCCATCG	59.96	154
	Reverse	CCAGTTGGTAACAATGCCATGT	59.44	
S100A9	Forward	GAAGCACAGTTGGCAACCTT	59.25	75
	Reverse	CAGGTCCTCCATGATGTCAT	56.68	
VEGF	Forward	CTGTGCAGGCTGCTGTAAC	59.13	184
	Reverse	ACAGTGATTTTCTGGCTTTGTTC	58.06	
ICAM-1	Forward	CTGAAAGATGAGCTCGAGAGTG	58.56	141
	Reverse	AAACGAATACACGGTGATGGTA	57.81	
TSP-1	Forward	TGTCCTGTTCCTGTTGCATA	56.76	422
	Reverse	CCAGGAGAGCTTCCTCCACT	60.62	

Institutes of Health, Baltimore, MD). β-Actin served as the loading control.

CCK-8 assay for cell viability: To assess the effects of $CoCl_2$-induced hypoxia and tasquinimod treatment on HREC viability, a cell counting kit-8 (CCK-8) assay was performed. HRECs in the logarithmic growth phase were collected and seeded into 96-well plates at a density of 5,000 cells per well with six replicates per condition, in a total volume of 200 µl per well. The cells were cultured under 37 °C, 5% CO_2, and saturated humidity conditions for 12 h or 24 h. At the time points (12 h and 24 h), 20 µl CCK-8 reagent was added to each well and incubated at 37 °C for 2 h. The absorbance was measured at 450 nm using a microplate reader after a color change from red to yellow, and statistical analysis was performed.

Statistical analysis: All experiments were performed in triplicate, and data are presented as mean ± standard deviation (SD). Statistical analyses were conducted using GraphPad Prism 5 (GraphPad Software, La Jolla, CA). For comparisons between two groups, an unpaired two-tailed Student *t* test was used. For comparisons among three or more groups, one-way analysis of variance (ANOVA) followed by post hoc test was performed. Additionally, for experiments involving two independent variables (e.g., different concentrations of $CoCl_2$ across multiple time points), a two-way ANOVA was applied to assess the effects of treatment, time, and their interaction. A p value of <0.05 was considered statistically significant (*$p < 0.05$, **$p < 0.01$, ***$p < 0.001$, and ****$p < 0.0001$).

RESULTS

Tasquinimod reduces retinal nonperfusion areas in OIR mice: To assess the effect of tasquinimod on ischemia-induced retinal neovascularization, a well-established OIR model was used [21]. Neonatal mice were exposed to 75% oxygen for 5 days (P7–P12) to induce vascular obliteration, followed by normoxic recovery (room air, 21% oxygen) from P12 to P17 to stimulate ischemia-induced retinal neovascularization (Figure 1A). Whole-mount isolectin B4 staining was performed to visualize retinal vasculature (Figure 1B), and the avascular area (nonperfusion region) was quantified as a percentage of total retinal area. To provide temporal context for disease progression, we included an OIR12 group representing the time point immediately after hyperoxic exposure and before neovascular responses begin. Although not directly used for treatment comparison, this group illustrates the transition between vessel obliteration and subsequent revascularization. Retinal flat-mount imaging revealed that OIR17 and OIR12 + PBS 5d contained prominent preretinal neovascular tufts with irregular, glomeruloid vessel clusters, whereas tasquinimod-treated retinas displayed a more uniform intraretinal capillary network with fewer preretinal tufts (Figure 1B). Consistent with these features, mice treated with tasquinimod from P12 to P17 exhibited significantly reduced avascular areas (9.62% ± 1.13%) compared to the OIR17 group (20.51% ± 0.93%) and the vehicle control group receiving PBS (20.27% ± 0.36%; $p < 0.001$; Figure 1C).

To further corroborate the revascularization and structural recovery of the retina, hematoxylin and eosin staining of retinal cross sections was performed at P17 (Figure 1D). Compared with the normal group, OIR17 sections exhibited disorganization of the inner retina (ganglion cell layer [GCL], inner nuclear layer [INL], inner plexiform layer (IPL), and inner nuclear layer [INL]) with focal preretinal cellular tufts and blurred laminar boundaries, consistent with hypoxia-driven neovascular changes [48]. The OIR12 + PBS 5d group showed persistent lamination irregularities with blurred INL–IPL boundaries and focal unevenness of the inner retina, compared with the normal group. In contrast, tasquinimod-treated retinas displayed more continuous lamination and fewer ectopic preretinal cellular clusters.

Taken together with the reduction in avascular area on flat-mounts, and given that retinal injury occurs during the P7 to P12 hyperoxic phase, these imaging and histologic findings indicate that tasquinimod primarily promotes intraretinal revascularization. This process, along with structural recovery and repair, occurs from P12 to P17, rather than preservation before injury.

Tasquinimod suppresses the expression of angiogenesis-related factors in the OIR retina: To investigate the molecular mechanism by which tasquinimod suppresses ischemia-induced retinal neovascularization in OIR mice, we evaluated the messenger RNA (mRNA) expression of angiogenesis-associated genes, including S100A9, VEGF, ICAM-1, and TSP-1 (Figure 2). Compared with the normal group, the OIR17 group (P17) exhibited significant upregulation of all four genes: S100A9 (3.00 ± 0.13), VEGF (2.49 ± 0.10), ICAM-1 (2.91 ± 0.38), and TSP-1 (2.60 ± 0.31). Oral administration of tasquinimod significantly reduced the expression of each factor compared with both the untreated OIR17 group and the OIR12 + PBS 5d control group ($p < 0.001$ for all comparisons), suggesting that the observed downregulation is a specific effect of tasquinimod rather than vehicle exposure. In contrast, the OIR12 + PBS 5d group did not show any significant differences from the untreated OIR17 group, supporting the specificity of tasquinimod's action. Western blot analysis corroborated the qPCR findings at the protein level (Figure 3). The OIR17 group exhibited marked increases in S100A9,

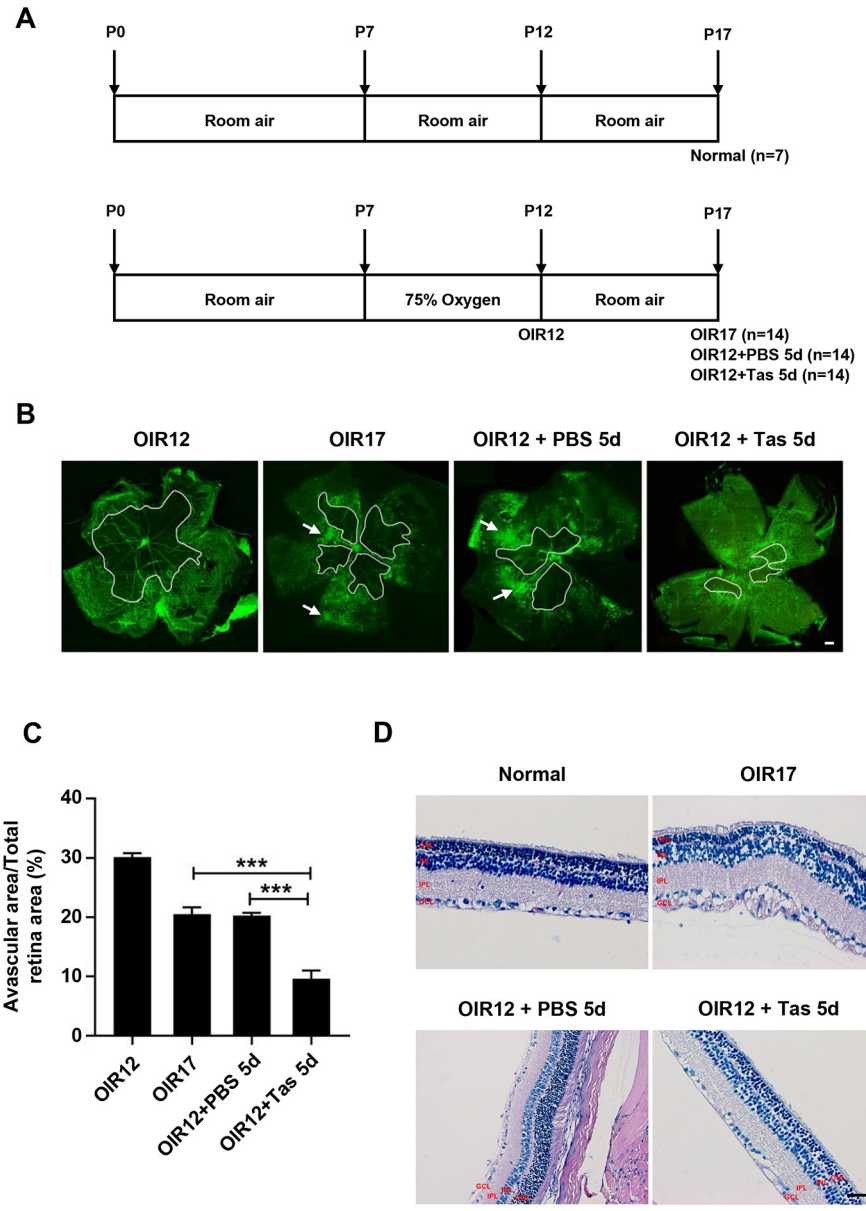


Figure 1. Tasquinimod reduces retinal nonperfusion areas and preserves retinal architecture in oxygen-induced retinopathy (OIR) mice. **A**: A schematic representation of the OIR model and experimental design is shown. The upper panel shows the normal group, and the lower panel illustrates the OIR group exposed to 75% oxygen from postnatal day (P) 7 to P12, followed by normoxia until P17. Tasquinimod (10 mg/kg/d) or phosphate-buffered saline (PBS) was administered by oral gavage from P12 to P17. **B**: Representative isolectin B4-stained whole-mount retinal images of the retinal vasculature are shown. The white-outlined regions indicate avascular areas. The scale bar represents 200 µm. **C**: The avascular area as a percentage of the total retinal area was quantified. Data are presented as the mean ± SD (n = 6 per group). A p value of less than 0.05 was considered statistically significant. ***p < 0.001. **D**: Representative hematoxylin and eosin-stained retinal cross-sections at P17 are shown for each group. The OIR17 group shows inner-retina disorganization with blurred GCL, IPL, and INL boundaries and focal preretinal cellular clusters. The OIR12 + PBS 5d group exhibits persistent lamination irregularities with indistinct INL–IPL demarcation and local unevenness of the inner retina. In contrast, the OIR12 + Tas 5d group displays more continuous lamination and fewer preretinal cellular clusters. GCL indicates ganglion cell layer; INL indicates inner nuclear layer; and ONL indicates outer nuclear layer. The scale bar represents 50 µm.

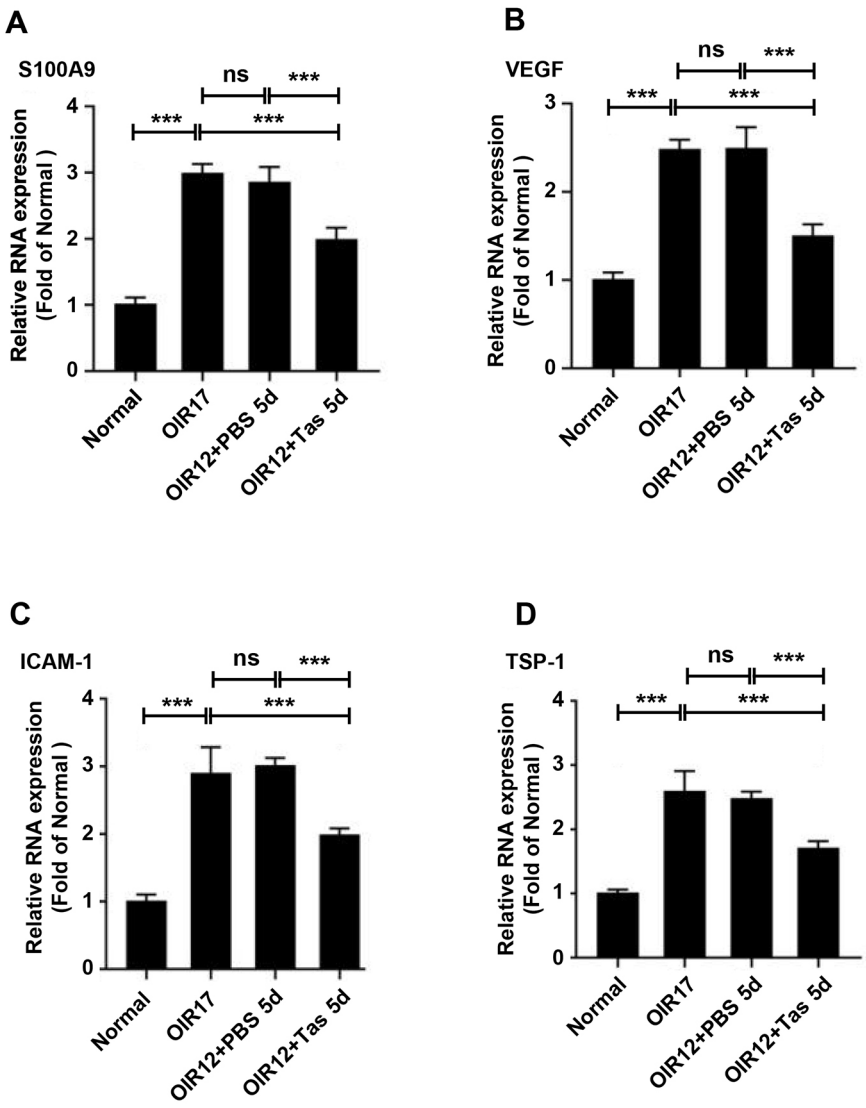


Figure 2. Tasquinimod suppresses angiogenesis-related gene expression in the oxygen-induced retinopathy (OIR) retina. Quantitative reverse transcription quantitative polymerase chain reaction (RT-qPCR) was performed to determine the relative mRNA expression levels of S100A9 (**A**), VEGF (**B**), ICAM-1 (**C**), and TSP-1 (**D**) in the normal, OIR17, OIR12 + PBS 5d, and OIR12 + Tas 5d groups. Expression levels were normalized to β-actin RNA. Data are presented as the mean ± SD (n = 6 per group). ***p < 0.001.

VEGF-A, ICAM-1, and TSP-1 expression compared to the normal group. Tasquinimod treatment significantly attenuated the expression of these proteins, reducing S100A9 by 38.4%, VEGF by 29.8%, ICAM-1 by 43.3%, and TSP-1 by 33.6% compared to the OIR + PBS 5d group ($p < 0.001$ for all). No significant difference was observed between OIR17 and OIR12 + PBS 5d groups, confirming that the therapeutic effect was not attributable to vehicle administration.

These findings demonstrate that tasquinimod effectively downregulates angiogenesis-related factors in the ischemic retina. This occurs potentially through inhibition of S100A9 signaling, thereby reducing retinal inflammation and pathological neovascularization.

Hypoxia induces upregulation of S100A9 in HRECs: To investigate the impact of hypoxia on S100A9 expression in HRECs, we used $CoCl_2$ to simulate hypoxic conditions. $CoCl_2$ is a well-established hypoxia-mimetic agent that stabilizes HIF-1α, leading to the activation of hypoxia-responsive pathways [45-47]. Before examining S100A9 regulation, we first assessed the effects of $CoCl_2$ exposure on cell viability using a CCK-8 assay. The results demonstrated that $CoCl_2$ reduced HREC viability in a dose- and time-dependent

manner. While short-term exposure (0–12 h) had minimal impact, prolonged hypoxia (24 h) significantly reduced cell viability, particularly at 200-µM and 300-µM concentrations (Figure 4A). This decline in cell survival suggests that sustained hypoxia impairs endothelial function, which may reflect the pathological state of ischemic retinal diseases.

Having established that $CoCl_2$-induced hypoxia alters HREC viability, we next examined its effect on S100A9 expression. HRECs were cultured under normoxic conditions or treated with 200 µM $CoCl_2$ for 24 h to induce hypoxia. RT-qPCR analysis revealed that, compared to the normoxic control, $CoCl_2$ treatment resulted in a significant increase in HIF-1α mRNA levels (approximately threefold) and S100A9 mRNA levels (approximately twofold; Figure 4B,C). Western blot analysis further confirmed that the protein levels of HIF-1α and S100A9 were markedly elevated under hypoxic conditions, with HIF-1α increasing by approximately 1.6-fold and S100A9 by approximately 1-fold compared to controls (Figure 4D–F). These findings suggest that hypoxia not only induces S100A9 expression in HRECs but may also contribute to endothelial dysfunction, as reflected by decreased cell viability under prolonged hypoxic conditions.

Tasquinimod suppresses the expression of angiogenesis-related factors in hypoxia-induced HRECs: To further investigate the impact of hypoxia and tasquinimod treatment on angiogenesis-related gene expression in HRECs, we first assessed the effects of tasquinimod treatment on cell viability using a CCK-8 assay. HRECs were cultured under normoxic conditions or exposed to 200 µM $CoCl_2$ for 24 h, with or without tasquinimod cotreatment. At 0 h, there were no significant differences in cell viability across all treatment groups. However, after 24 h of hypoxia, 5 µM tasquinimod significantly improved cell viability compared to the hypoxia-only group, suggesting that tasquinimod may mitigate hypoxia-induced cytotoxicity (Figure 5A). Importantly, tasquinimod alone (5 µM) did not affect cell viability,

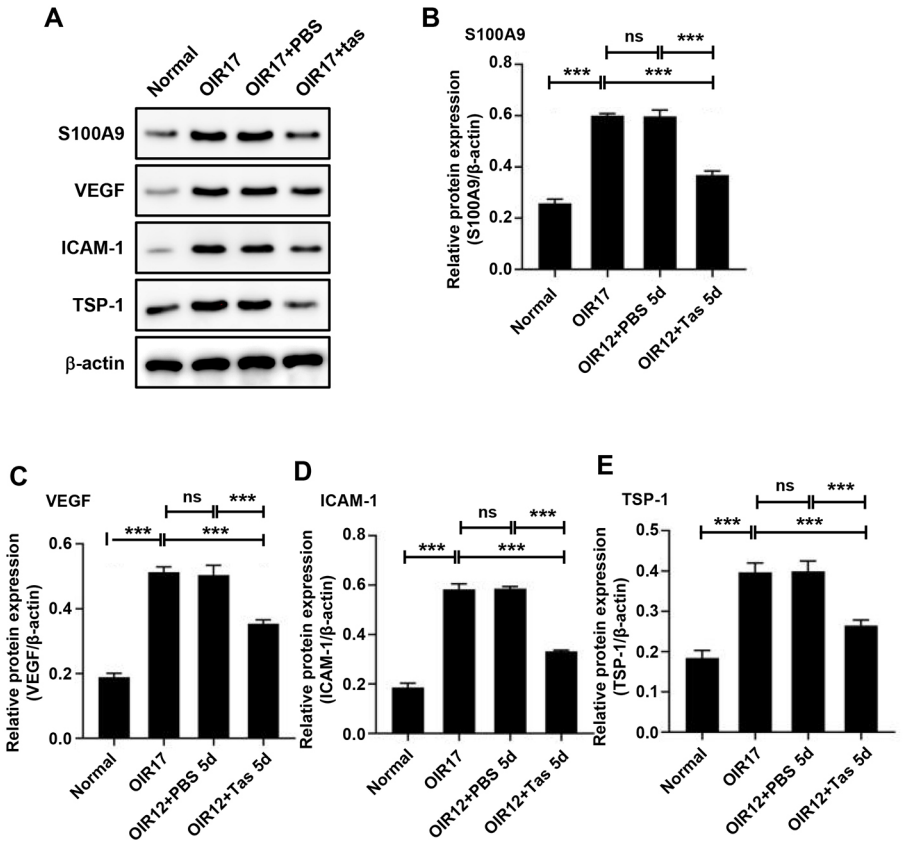


Figure 3. Tasquinimod suppresses angiogenesis-related protein expression in the oxygen-induced retinopathy (OIR) retina. **A**: Representative western blots show the protein expression of S100A9, VEGF, ICAM-1, and TSP-1 in the normal, OIR17, OIR12 + PBS 5d, and OIR12 + Tas 5d groups. Protein levels of S100A9 (**B**), VEGF (**C**), ICAM-1 (D), and TSP-1 (**E**) were quantified and normalized to β-actin. Data are presented as the mean ± SD (n = 6 per group). ***p < 0.001.

as there was no significant difference between the untreated control (HREC) and HREC + 5 μM tasquinimod group. This confirms that tasquinimod does not exert cytotoxic effects at the tested concentrations, further supporting its safety profile in retinal endothelial cells. However, while tasquinimod partially rescued cell viability under hypoxia, it did not completely restore viability to normoxic levels, indicating that additional mechanisms may contribute to hypoxia-induced cell damage beyond S100A9 inhibition.

We then performed RT-qPCR to evaluate whether tasquinimod modulates the expression of angiogenesis-related genes under hypoxic conditions. HRECs were divided into four groups: normal (normoxia), hypoxia (200 μM $CoCl_2$), hypoxia + 1 μM tasquinimod, and hypoxia + 5 μM

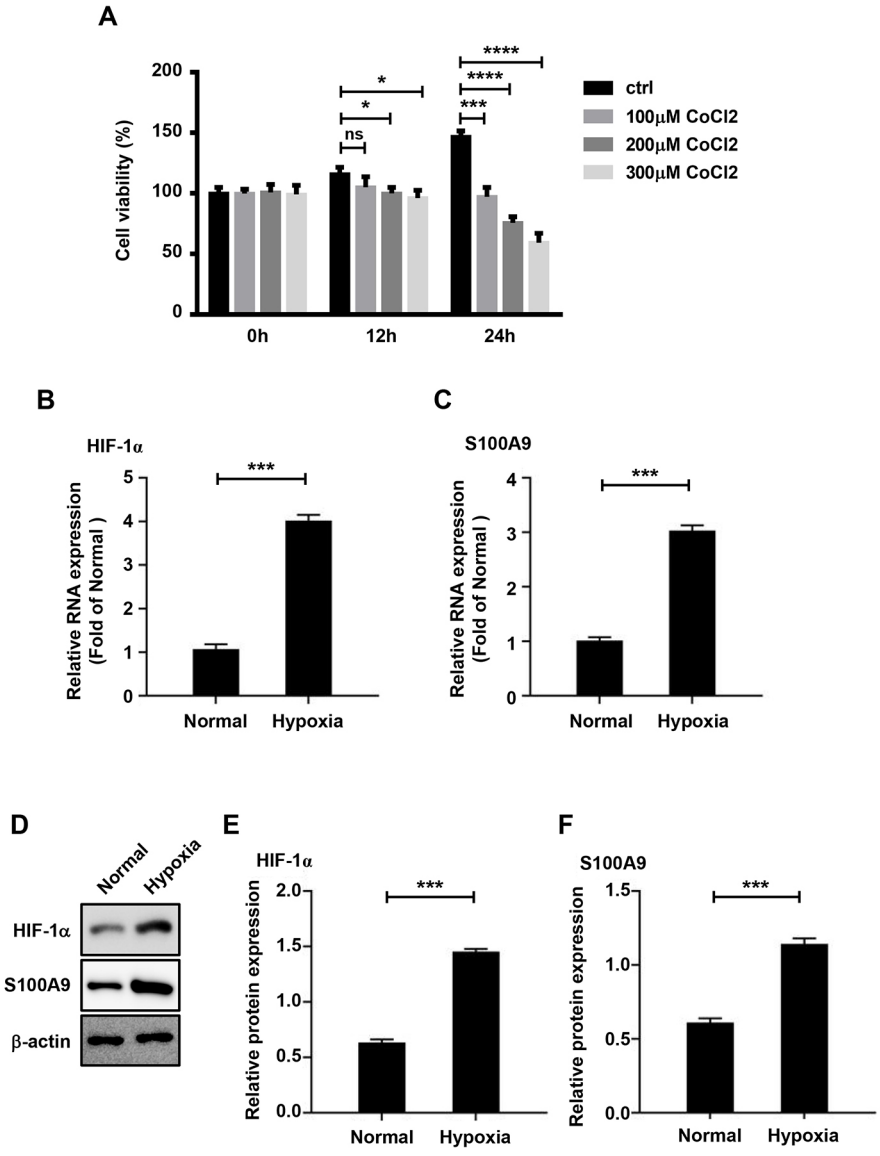


Figure 4. Hypoxia induces HIF-1α and S100A9 expression in human retinal capillary endothelial cells (HRECs). **A**: A CCK-8 assay was performed to assess HREC viability after treatment with 100 μM, 200 μM, or 300 μM cobalt chloride (CoCl2) for 12 h and 24 h. Data are presented as a percentage of the control at 0 h. Quantitative reverse transcription quantitative polymerase chain reaction analysis was performed to determine HIF-1α (**B**) and S100A9 (**C**) mRNA expression under normoxia or 200 μM CoCl2-induced hypoxia, with normalization to β-actin. **D**: Representative western blots show HIF-1α and S100A9 protein expression in HRECs under normoxic and hypoxic conditions. Protein levels of HIF-1α (**E**) and S100A9 (**F**) are expressed as the ratio of target protein expression to β-actin. Data are presented as the mean ± SD. ***p < 0.001 and ****p < 0.0001.

tasquinimod. RT-qPCR analysis revealed that hypoxia significantly upregulated the mRNA expression levels of HIF-1α, VEGF, ICAM-1, and TSP-1, with HIF-1α increasing approximately 3.91-fold, VEGF by 1.50-fold, ICAM-1 by 2.86-fold, and TSP-1 by 1.98-fold compared to the normal control. Treatment with 1 μM tasquinimod markedly reduced the expression of these genes, while 5 μM tasquinimod

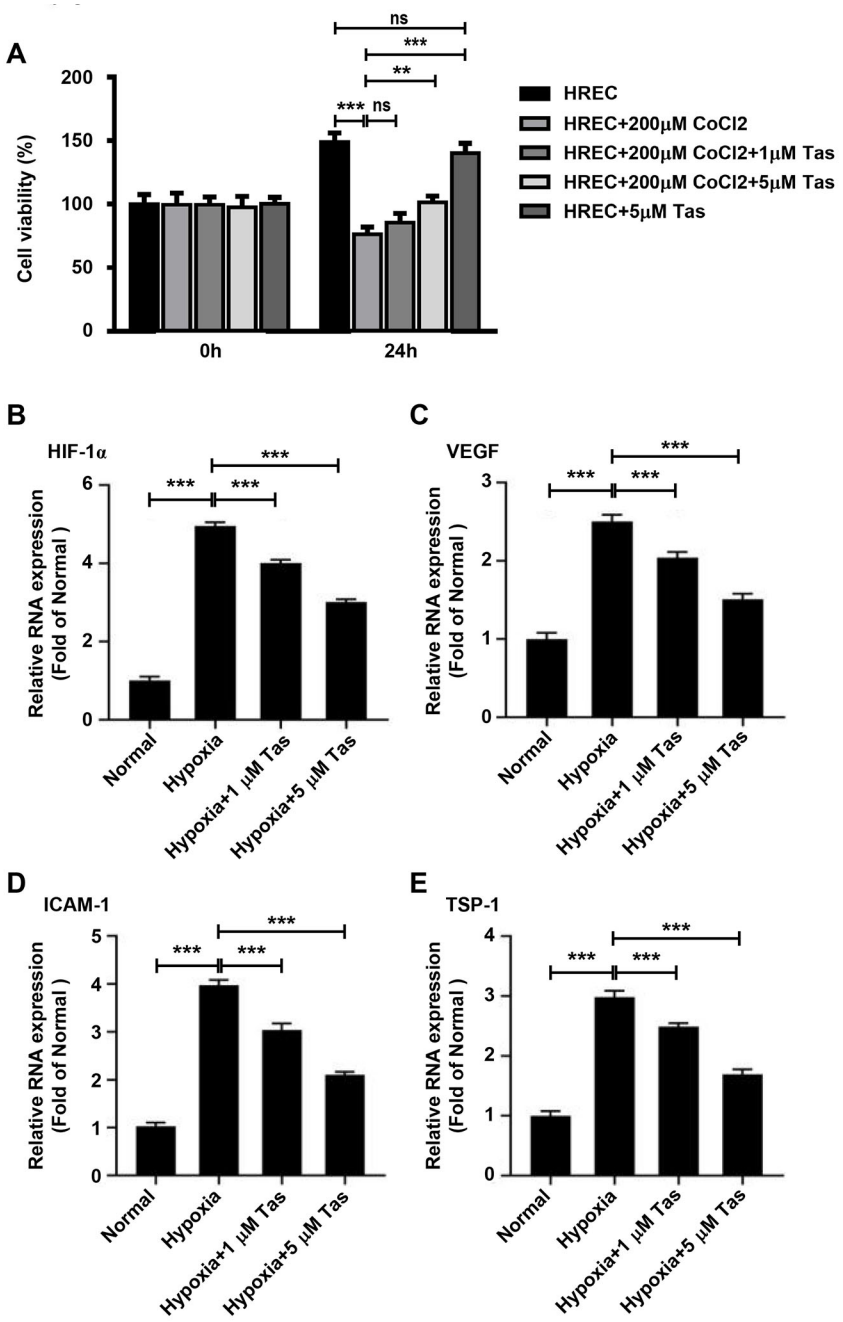


Figure 5. Tasquinimod suppresses angiogenesis-related gene expression in hypoxia-stimulated human retinal capillary endothelial cells (HRECs). **A**: A CCK-8 assay was performed to assess cell viability under 200 μM cobalt chloride (CoCl2)-induced hypoxia with or without tasquinimod (1 μM or 5 μM) for 24 h. Data are presented as the percentage of the HREC group at 0 h. Quantitative reverse transcription quantitative polymerase chain reaction analysis was performed to determine the relative messenger RNA expression levels of HIF-1α (**B**), VEGF (**C**), ICAM-1 (**D**), and TSP-1 (**E**), with normalization to β-actin. Data are presented as the mean ± SD. **p < 0.01, ***p < 0.001. ns indicates no significant difference.

further suppressed hypoxia-induced upregulation, indicating a dose-dependent inhibitory effect (Figure 5B–E).

To further validate the impact of tasquinimod on hypoxia-induced angiogenic factor expression, we performed western blot analysis to assess the protein levels of HIF-1α, VEGF, ICAM-1, and TSP-1 in HRECs under the same conditions. Consistent with the qPCR findings, hypoxia significantly upregulated the protein expression of all these factors compared to the normoxic group. Treatment with 1 μM tasquinimod resulted in a notable reduction in the expression of these proteins, while 5 μM tasquinimod led to an even more pronounced suppression, suggesting a dose-dependent inhibitory effect (Figure 6).

Tasquinimod inhibits hypoxia-induced migration and tube formation of HRECs: Endothelial cell migration is a crucial process in angiogenesis, facilitating new vessel sprouting and tissue remodeling [49]. To investigate the effect of tasquinimod on hypoxia-induced endothelial cell migration, we performed a Transwell migration assay. As shown in Figure 7, hypoxia significantly enhanced the migration of HRECs compared to the normal condition. However, treatment with 1 μM tasquinimod notably suppressed cell migration, and this inhibitory effect was further enhanced by 5 μM tasquinimod. These findings suggest that tasquinimod effectively inhibits endothelial migration under hypoxic conditions.

To further evaluate the antiangiogenic effect of tasquinimod, we conducted a Matrigel tube formation assay. Hypoxic conditions markedly enhanced tube formation, as evidenced by a significant increase in the number of junctions (Figure 8B) and total branching length (Figure 8C) compared to the normoxia group. Treatment with 1 μM tasquinimod significantly attenuated these effects, and 5 μM tasquinimod led to further reductions in both junction number and branching length. These results demonstrate that tasquinimod

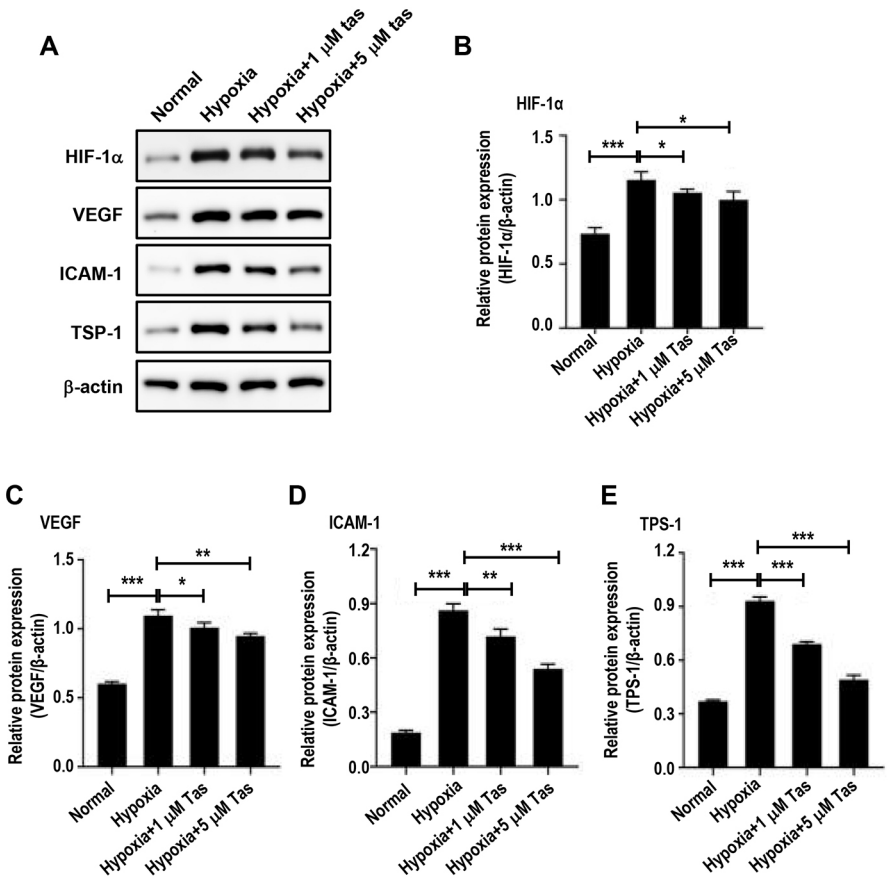


Figure 6. Tasquinimod suppresses angiogenesis-related protein expression in hypoxia-stimulated human retinal capillary endothelial cells (HRECs). **A**: Representative western blot images show the expression levels of HIF-1α, VEGF, ICAM-1, and TSP-1 in HRECs under normoxic or hypoxic conditions, with or without tasquinimod treatment. Protein levels of HIF-1α (**B**), VEGF (**C**), ICAM-1 (**D**), and TSP-1 (**E**) were quantified and normalized to β-actin. Data are presented as the mean ± SD. ***p < 0.001.

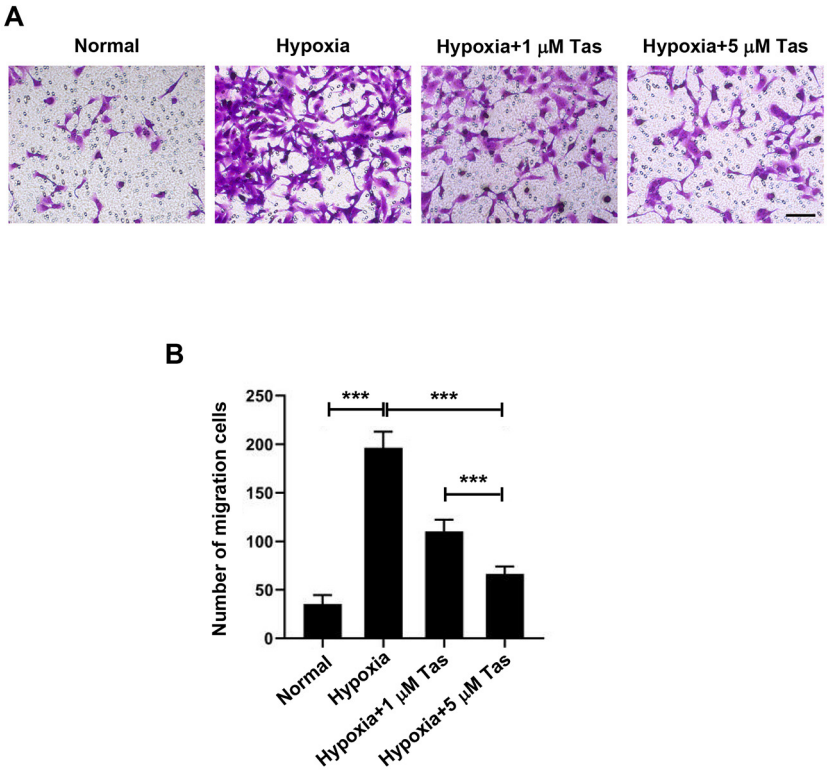


Figure 7. Tasquinimod inhibits hypoxia-induced migration of human retinal capillary endothelial cells (HRECs). **A**: Representative images show migrated HRECs stained with crystal violet under normoxic or hypoxic conditions, with or without tasquinimod treatment. The scale bar represents 200 μm. **B**: The number of migrated cells in each group was quantified. Data are presented as the mean ± SD. ***p < 0.001.

suppresses key functional processes involved in angiogenesis—including endothelial migration and capillary-like network formation—under hypoxic conditions, supporting its potential role as an antiangiogenic agent.

DISCUSSION

Retinal neovascularization, a hallmark of ischemic retinopathies such as ROP, DR, and RVO, involves both aberrant angiogenesis and chronic inflammation driven by hypoxic stress [50-52]. In this study, we demonstrated that the inflammatory mediator S100A9 is upregulated in the ischemic retina of OIR mice and in hypoxia-stimulated retinal endothelial cells. Pharmacological inhibition of S100A9 using tasquinimod [36] led to a significant reduction in nonperfusion areas and downregulation of key angiogenesis- and inflammation-related factors, including VEGF, ICAM-1, and TSP-1. These findings support the concept that S100A9 contributes to hypoxia-induced vascular dysfunction and that its inhibition offers a novel anti-inflammatory and antiangiogenic strategy for ischemic retinal diseases. Moreover, histologic assessment of P17 retinal sections was consistent with these findings. Relative to the OIR17 and OIR12 + PBS 5d group, tasquinimod-treated retinas exhibited more continuous lamination (clearer GCL, IPL, and INL boundaries) with fewer preretinal nuclei on the vitreous side. Although not quantified, these qualitative differences indicate improved inner-retina organization in the treated group.

In the OIR paradigm, return to room air after hyperoxia leads to two separable vascular outcomes: pathological preretinal neovascularization (tufts) and physiological intraretinal revascularization of avascular zones [13,44]. In our data, tasquinimod reduced the nonperfused area from P12 to P17, and the flat-mounts showed fewer preretinal tufts with a more uniform intraretinal capillary network (Figure 1B,C). Consistently, cross sections revealed fewer preretinal nuclei and more continuous inner-retina lamination after tasquinimod (Figure 1D). Thus, the smaller avascular areas at P17 most likely reflect improved physiological revascularization, while the concomitant suppression of VEGF and ICAM-1 (Figure 2, Figure 3) indicates attenuation of inflammation-driven pathological sprouting [53-56]. This pattern is compatible with a vascular-normalization framework, in which limiting inflammatory, disorganized tuft formation permits or even facilitates orderly intraretinal

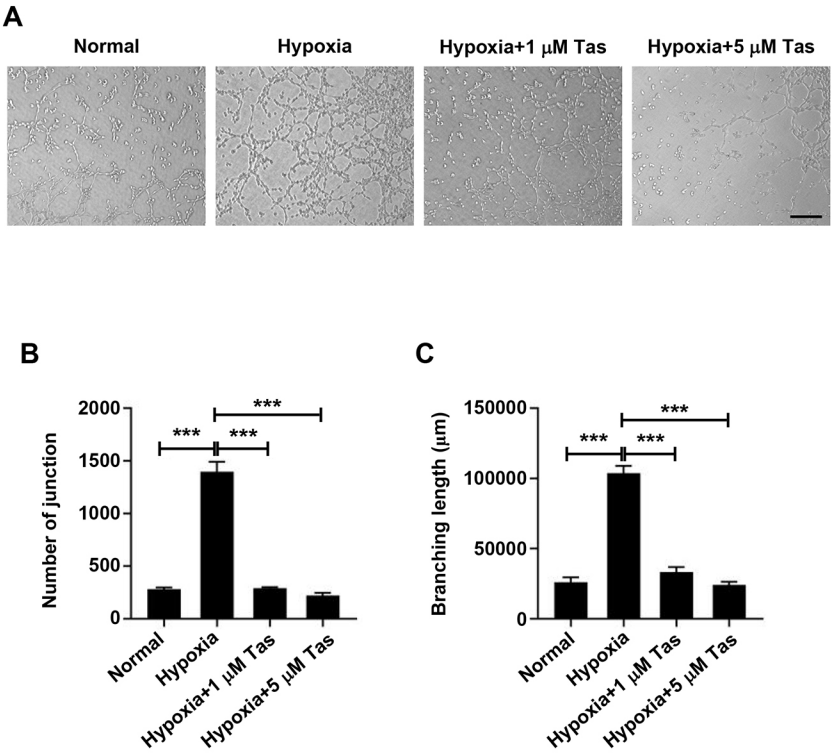


Figure 8. Tasquinimod inhibits hypoxia-induced tube formation of human retinal capillary endothelial cells (HRECs). **A**: Representative images show tube formation by HRECs under normoxic or hypoxic conditions, with or without tasquinimod treatment. The scale bar represents 200 μm. The number of junctions (**B**) and total branching length (C) were quantified. Data are presented as the mean ± SD. ***p < 0.001.

revascularization and perfusion recovery [57,58]. Finally, because tasquinimod targets the S100A9 axis, which is implicated in retinal inflammation and endothelial activation [27,40,59], its anti-inflammatory action provides a plausible mechanistic basis for reducing pathological tufts while allowing physiological capillary regrowth.

Importantly, the timing of tasquinimod administration differed between our two experimental arms. In the OIR model, the drug was started after the hyperoxia-induced injury window and given throughout P12 to P17, thereby probing postinsult recovery. By contrast, in HRECs, tasquinimod was applied concurrently with hypoxic stimulation, modeling an early or coincident intervention. This difference helps explain why cell assays show more immediate molecular changes, whereas the in vivo readouts emphasize revascularization and structural recovery. To bridge these designs, future OIR studies will vary the initiation window (e.g., P7, P12, P14) and compare effects on avascular area, tuft area, and intraretinal revascularization, together with molecular endpoints (VEGF, ICAM-1, and S100A9).

This study addresses a gap in the current literature by linking S100A9 inhibition to the suppression of pathological angiogenesis in a hypoxic retinal context. Previous clinical and experimental studies have established S100A9 as a DAMP protein involved in leukocyte activation and vascular inflammation [60,61]. For example, elevated S100A9 levels have been observed in the vitreous fluid of patients with proliferative diabetic retinopathy [35], supporting its role in ocular inflammation. In addition, members of the S100 protein family have been implicated in various ocular diseases involving neovascularization or vascular dysfunction, such as age-related macular degeneration and central retinal vein occlusion [62,63], although not all are strictly ischemia-driven. However, no prior study has specifically evaluated the therapeutic effects of an S100A9 inhibitor in ischemia-driven retinal neovascularization. Our findings extend previous observations by demonstrating that

tasquinimod not only reduces S100A9 expression under hypoxia but also suppresses angiogenic and inflammatory pathways.

Mechanistically, we observed that tasquinimod downregulated VEGF and ICAM-1 expression in both OIR retinas and hypoxia-treated HRECs. VEGF is a well-characterized target in retinal vascular diseases. Although anti-VEGF agents such as ranibizumab and aflibercept have demonstrated clinical efficacy, their therapeutic effects are transient, necessitating repeated intravitreal injections [64,65]. Additionally, these treatments may be associated with ocular inflammatory responses, such as intraocular inflammation and retinal vasculitis [66,67]. Moreover, their ability to reverse capillary nonperfusion remains uncertain and is subject to ongoing investigation [68-71]. In contrast, S100A9 inhibition may affect upstream inflammatory signaling, thereby offering a complementary therapeutic mechanism. Nevertheless, due to the absence of direct comparison with anti-VEGF agents in our study, the relative efficacy and potential additive benefit of tasquinimod require further investigation.

Tasquinimod also reduced TSP-1 expression under hypoxia, a finding that may appear paradoxical given TSP-1's known antiangiogenic role. However, prior studies have shown that TSP-1 expression increases during the neovascular phase in the OIR model, potentially as a reactive response to VEGF elevation [72]. The observed TSP-1 downregulation may therefore reflect an overall amelioration of hypoxia rather than a direct anti-TSP effect. These results highlight the need to further delineate the signaling hierarchy between S100A9, VEGF, and TSP-1. While tasquinimod is a well-characterized inhibitor of the S100A9 axis, context-specific causal evidence in our HREC system is still required. To address this, future work will incorporate exogenous S100A8/A9 dose–response assays in HRECs to directly test whether tasquinimod antagonizes S100-driven NF-κB activation and ICAM-1/VEGF induction, thereby establishing a causal link between the S100A9 pathway and the observed protective effects.

Despite these findings, our study has several limitations. First, we used only a single in vivo dosage (10 mg/kg tasquinimod) and a single time point (P17) to assess therapeutic efficacy in the OIR model. A more comprehensive dose–response analysis and longitudinal evaluation would better characterize the pharmacodynamics and potential toxicity. Second, we did not include comparator groups treated with anti-VEGF agents such as ranibizumab or aflibercept, precluding conclusions regarding tasquinimod's relative efficacy or combinatorial value. Third, while tasquinimod is known to inhibit S100A9, our data do not establish a causal relationship between S100A9 suppression and the observed vascular improvements. Functional validation using S100A9 knockdown, overexpression, or neutralizing antibodies would provide stronger mechanistic evidence. Finally, we assessed a limited number of angiogenesis and inflammation markers. Unbiased transcriptomic profiling (e.g., RNA sequencing) or proteomic approaches may uncover additional tasquinimod-regulated targets and broaden the mechanistic landscape.

Conclusion: This study demonstrates that tasquinimod attenuates ischemia-induced retinal neovascularization and inflammation, potentially via suppression of S100A9 signaling. By downregulating VEGF, ICAM-1, and TSP-1, tasquinimod modulates key pathways involved in endothelial activation and angiogenesis. These results suggest that targeting S100A9 may represent a novel therapeutic strategy for ischemic retinopathies. Future investigations should validate the specificity and durability of this effect in chronic disease models, compare tasquinimod with current standard-of-care therapies, and explore its clinical applicability in ROP, DR, and RVO.

ACKNOWLEDGMENTS

Author Contribution Conceptualization: Ji Jin Data curation: Fangfang Ji Formal Analysis: Fangfang Ji Funding acquisition: Ji Jin Investigation: Ji Jin Methodology: Ji Jin Project administration: Fangfang Ji Resources: Ji Jin Software: Fangfang Ji Supervision: Ji Jin Validation: Ji Zhang Visualization: Ji Zhang Writing – original draft: Fangfang Ji Writing – review & editing: Ji Jin Conflict of interest statement None declared This study was supported by the Suzhou Science and Technology Fund of China (SYS2020137).

This is an open-access article distributed under the terms of the Creative Commons Attribution-NonCommercial-NoDerivatives 4.0 International License, which permits reusers to copy and distribute the material in any medium or format in unadapted form only, for noncommercial purposes only, and only so long as attribution is given to the creator. CC BY-NC-ND includes the following elements: BY: credit must be given to the creator. NC: Only noncommercial uses of the work are permitted. ND: No derivatives or adaptations of the work are permitted

REFERENCES

1. Hong EH, Shin YU, Cho H. Retinopathy of prematurity: a review of epidemiology and current treatment strategies. Clin Exp Pediatr 2022; 65:115-26. [PMID: 34645255].

2. Jia Y, Xue W, Tong X, Wang Y, Cui L, Zou H. Quantitative analysis and clinical application of iris circulation in ischemic retinal disease. BMC Ophthalmol 2021; 21:393-[PMID: 34781913].

3. Yau JW, Rogers SL, Kawasaki R, Lamoureux EL, Kowalski JW, Bek T, Chen SJ, Dekker JM, Fletcher A, Grauslund J, Haffner S, Hamman RF, Ikram MK, Kayama T, Klein BE, Klein R, Krishnaiah S, Mayurasakorn K, O'Hare JP, Orchard TJ, Porta M, Rema M, Roy MS, Sharma T, Shaw J, Taylor H, Tielsch JM, Varma R, Wang JJ, Wang N, West S, Xu L, Yasuda M, Zhang X, Mitchell P, Wong TY. Meta-Analysis for Eye Disease (META-EYE) Study Group. Global prevalence and major risk factors of diabetic retinopathy. Diabetes Care 2012; 35:556-64. [PMID: 22301125].

4. Whiting DR, Guariguata L, Weil C, Shaw J. IDF diabetes atlas: global estimates of the prevalence of diabetes for 2011 and 2030. Diabetes Res Clin Pract 2011; 94:311-21. [PMID: 22079683].

5. Song P, Xu Y, Zha M, Zhang Y, Rudan I. Global epidemiology of retinal vein occlusion: a systematic review and meta-analysis of prevalence, incidence, and risk factors. J Glob Health 2019; 9:010427[PMID: 31131101].

6. Zhang RH, Liu YM, Dong L, Li HY, Li YF, Zhou WD, Wu HT, Wang YX, Wei WB. Prevalence, Years Lived With Disability, and Time Trends for 16 Causes of Blindness and Vision Impairment: Findings Highlight Retinopathy of Prematurity. Front Pediatr 2022; 10:735335[PMID: 35359888].

7. Lee D, Tomita Y, Miwa Y, Kunimi H, Nakai A, Shoda C, Negishi K, Kurihara T. Recent Insights into Roles of Hypoxia-Inducible Factors in Retinal Diseases. Int J Mol Sci 2024; 25:10140-[PMID: 39337623].

8. Belokopytov M, Belkin M, Dubinsky G, Epstein Y, Rosner M. Development and recovery of laser-induced retinal lesion in rats. Retina 2010; 30:662-70. [PMID: 19996833].

9. Fong DS, Girach A, Boney A. Visual side effects of successful scatter laser photocoagulation surgery for proliferative diabetic retinopathy: a literature review. Retina 2007; 27:816-24. [PMID: 17891003].

10. Yu PK, Cringle SJ, McAllister IL, Yu DY. Low power laser treatment of the retina ameliorates neovascularisation in a transgenic mouse model of retinal neovascularisation. Exp Eye Res 2009; 89:791-800. [PMID: 19615996].

11. Eng VA, Rayess N, Nguyen HV, Leng T. Complete RPE and outer retinal atrophy in patients receiving anti-VEGF treatment for neovascular age-related macular degeneration. PLoS One 2020; 15:e0232353[PMID: 32369500].

12. Xu M, Fan R, Fan X, Shao Y, Li X. Progress and Challenges of Anti-VEGF Agents and Their Sustained-Release Strategies for Retinal Angiogenesis. Drug Des Devel Ther 2022; 16:3241-62. [PMID: 36172053].

13. Scott A, Fruttiger M. Oxygen-induced retinopathy: a model for vascular pathology in the retina. Eye (Lond) 2010; 24:416-21. [PMID: 20010791].

14. Quiroz J, Yazdanyar A. Animal models of diabetic retinopathy. Ann Transl Med 2021; 9:1272-[PMID: 34532409].

15. Foell D, Wittkowski H, Vogl T, Roth J. S100 proteins expressed in phagocytes: a novel group of damage-associated molecular pattern molecules. J Leukoc Biol 2007; 81:28-37. [PMID: 16943388].

16. Bianchi ME. DAMPs, PAMPs and alarmins: all we need to know about danger. J Leukoc Biol 2007; 81:1-5. [PMID: 17032697].

17. Srikrishna G, Freeze HH. Endogenous damage-associated molecular pattern molecules at the crossroads of inflammation and cancer. Neoplasia 2009; 11:615-28. [PMID: 19568407].

18. Zhao F, Hoechst B, Duffy A, Gamrekelashvili J, Fioravanti S, Manns MP, Greten TF, Korangy F. S100A9 a new marker for monocytic human myeloid-derived suppressor cells. Immunology 2012; 136:176-83. [PMID: 22304731].

19. Crowe LAN, McLean M, Kitson SM, Melchor EG, Patommel K, Cao HM, Reilly JH, Leach WJ, Rooney BP, Spencer SJ, Mullen M, Chambers M, Murrell GAC, McInnes IB, Akbar M, Millar NL. S100A8 & S100A9: Alarmin mediated inflammation in tendinopathy. Sci Rep 2019; 9:1463-[PMID: 30728384].

20. Eksioglu EA, Wright GM, Foulks JM, Lalonde M, Warner SL, Wright KL. Improvement of hematopoiesis in primary low risk MDS with the TGFBR1 investigational inhibitor TP-6379. [abstract]. In: Proceedings of the American Association for Cancer Research Annual Meeting 2023; Part 1 (Regular and Invited Abstracts); 2023 Apr 14-19; Orlando, FL. Philadelphia (PA): AACR; Cancer Res 2023;83(7_Suppl):Abstract nr 5150.

21. Jin J, Chen L, Liu GQ, Lu PR. Proteomic analysis of anti-angiogenic effects by conbercept in the mice with oxygen induced retinopathy. Int J Ophthalmol 2020; 13:1844-53. [PMID: 33344181].

22. Riva M, Källberg E, Björk P, Hancz D, Vogl T, Roth J, Ivars F, Leanderson T. Induction of nuclear factor-κB responses by the S100A9 protein is Toll-like receptor-4-dependent. Immunology 2012; 137:172-82. [PMID: 22804476].

23. Simard JC, Girard D, Tessier PA. Induction of neutrophil degranulation by S100A9 via a MAPK-dependent mechanism. J Leukoc Biol 2010; 87:905-14. [PMID: 20103766].

24. Viemann D, Strey A, Janning A, Jurk K, Klimmek K, Vogl T, Hirono K, Ichida F, Foell D, Kehrel B, Gerke V, Sorg C, Roth J. Myeloid-related proteins 8 and 14 induce a specific inflammatory response in human microvascular endothelial cells. Blood 2005; 105:2955-62. [PMID: 15598812].

25. Wang S, Song R, Wang Z, Jing Z, Wang S, Ma J. S100A8/A9 in Inflammation. Front Immunol 2018; 9:1298-[PMID: 29942307].

26. Zhong X, Xie F, Chen L, Liu Z, Wang Q. S100A8 and S100A9 promote endothelial cell activation through the RAGE-mediated mammalian target of rapamycin complex 2 pathway. Mol Med Rep 2020; 22:5293-303. [PMID: 33174028].

27. Wang L, Luo H, Chen X, Jiang Y, Huang Q. Functional characterization of S100A8 and S100A9 in altering monolayer permeability of human umbilical endothelial cells. PLoS One 2014; 9:e90472[PMID: 24595267].

28. Li C, Li S, Jia C, Yang L, Song Z, Wang Y. Low concentration of S100A8/9 promotes angiogenesis-related activity of vascular endothelial cells: bridges among inflammation, angiogenesis, and tumorigenesis? Mediators Inflamm 2012; 2012:248574[PMID: 22685372].

29. Kopeć-Mędrek M, Widuchowska M, Kucharz EJ. Calprotectin in rheumatic diseases: a review. Reumatologia 2016; 54:306-9. [PMID: 28115781].

30. Manolakis AC, Kapsoritakis AN, Tiaka EK, Potamianos SP. Calprotectin, calgranulin C, and other members of the s100 protein family in inflammatory bowel disease. Dig Dis Sci 2011; 56:1601-11. [PMID: 21203903].

31. Lylloff L, Bathum L, Madsbad S, Grundtvig JLG, Nordgaard-Lassen I, Fenger M. S100A8/A9 (Calprotectin), Interleukin-6, and C-Reactive Protein in Obesity and Diabetes before and after Roux-en-Y Gastric Bypass Surgery. Obes Facts 2017; 10:386-95. [PMID: 28848164].

32. Cheng G, He T, Xing Y. Silencing of S100A4, a metastasis-associated protein, inhibits retinal neovascularization via the downregulation of BDNF in oxygen-induced ischaemic retinopathy. Eye (Lond) 2016; 30:877-87. [PMID: 26987588].

33. Cheng G, Tian K, Zhang L, Yang N, Xing Y, He T. S100A4 gene silencing in oxygen-induced ischemic retinopathy inhibits retinal neovascularization via down-regulation of CREB expression. Graefes Arch Clin Exp Ophthalmol 2016; 254:97-108. [PMID: 26358273].

34. Tong L, Lan W, Lim RR, Chaurasia SS. S100A proteins as molecular targets in the ocular surface inflammatory diseases. Ocul Surf 2014; 12:23-31. [PMID: 24439044].

35. Abu El-Asrar AM, Alam K, Siddiquei MM, Van den Eynde K, Mohammad G, De Hertogh G, Opdenakker G. Myeloid-Related Protein-14/MRP-14/S100A9/Calgranulin B is Associated with Inflammation in Proliferative Diabetic Retinopathy. Ocul Immunol Inflamm 2018; 26:615-24. [PMID: 27849448].

36. Björk P, Björk A, Vogl T, Stenström M, Liberg D, Olsson A, Roth J, Ivars F, Leanderson T. Identification of human S100A9 as a novel target for treatment of autoimmune disease via binding to quinoline-3-carboxamides. PLoS Biol 2009; 7:e97[PMID: 19402754].

37. Fan R, Satilmis H, Vandewalle N, Verheye E, Vlummens P, Maes A, Muylaert C, De Bruyne E, Menu E, Evans H, Chantry A, De Beule N, Hose D, Törngren M, Eriksson H, Vanderkerken K, Maes K, Breckpot K, De Veirman K. Tasquinimod suppresses tumor cell growth and bone resorption by targeting immunosuppressive myeloid cells and inhibiting c-MYC expression in multiple myeloma. J Immunother Cancer 2023; 11:e005319[PMID: 36650020].

38. Isaacs JT, Pili R, Qian DZ, Dalrymple SL, Garrison JB, Kyprianou N, Björk A, Olsson A, Leanderson T. Identification of ABR-215050 as lead second generation quinoline-3-carboxamide anti-angiogenic agent for the treatment of prostate cancer. Prostate 2006; 66:1768-78. [PMID: 16955399].

39. Isaacs JT, Antony L, Dalrymple SL, Brennen WN, Gerber S, Hammers H, Wissing M, Kachhap S, Luo J, Xing L, Björk P, Olsson A, Björk A, Leanderson T. Tasquinimod Is an Allosteric Modulator of HDAC4 survival signaling within the compromised cancer microenvironment. Cancer Res 2013; 73:1386-99. [PMID: 23149916].

40. Jin J, Zhang J, Bu S. Tasquinimod efficacy and S100A9 expression in glucose-treated HREC cells. Int Ophthalmol 2022; 42:661-76. [PMID: 34796432].

41. Olsson A, Björk A, Vallon-Christersson J, Isaacs JT, Leanderson T. Tasquinimod (ABR-215050), a quinoline-3-carboxamide anti-angiogenic agent, modulates the expression of thrombospondin-1 in human prostate tumors. Mol Cancer 2010; 9:107-[PMID: 20470445].

42. Smith LE, Wesolowski E, McLellan A, Kostyk SK, D'Amato R, Sullivan R, D'Amore PA. Oxygen-induced retinopathy in the mouse. Invest Ophthalmol Vis Sci 1994; 35:101-11. [PMID: 7507904].

43. Tual-Chalot S, Allinson KR, Fruttiger M, Arthur HM. Whole mount immunofluorescent staining of the neonatal mouse retina to investigate angiogenesis in vivo. J Vis Exp 2013; 77e50546[PMID: 23892721].

44. Connor KM, Krah NM, Dennison RJ, Aderman CM, Chen J, Guerin KI, Sapieha P, Stahl A, Willett KL, Smith LE. Quantification of oxygen-induced retinopathy in the mouse: a model of vessel loss, vessel regrowth and pathological angiogenesis. Nat Protoc 2009; 4:1565-73. [PMID: 19816419].

45. Di Mattia M, Mauro A, Delle Monache S, Pulcini F, Russo V, Berardinelli P, Citeroni MR, Turriani M, Peserico A, Barboni B. Hypoxia-Mimetic $CoCl_2$ Agent Enhances Pro-Angiogenic Activities in Ovine Amniotic Epithelial Cells-Derived Conditioned Medium. Cells 2022; 11:461-[PMID: 35159271].

46. Li Q, Ma R, Zhang M. $CoCl_2$ increases the expression of hypoxic markers HIF-1α, VEGF and CXCR4 in breast cancer MCF-7 cells. Oncol Lett 2018; 15:1119-24. [PMID: 29391899].

47. Zhang YB, Wang X, Meister EA, Gong KR, Yan SC, Lu GW, Ji XM, Shao G. The effects of CoCl2 on HIF-1α protein under experimental conditions of autoprogressive hypoxia using mouse models. Int J Mol Sci 2014; 15:10999-1012. [PMID: 24945310].

48. Juan SCE, Palomares T, García-Alonso I, Herrero de la Parte B. Histological Assessment of Rat Retinas with Ischemia-Reperfusion Injury. Eur Surg Res 2021; 62:144-50. .

49. Lamalice L, Le Boeuf F, Huot J. Endothelial cell migration during angiogenesis. Circ Res 2007; 100:782-94. [PMID: 17395884].

50. Aouiss A, Anka Idrissi D, Kabine M, Zaid Y. Update of inflammatory proliferative retinopathy: Ischemia, hypoxia and angiogenesis. Curr Res Transl Med 2019; 67:62-71. [PMID: 30685380].

51. Ehlken C, Grundel B, Michels D, Junker B, Stahl A, Schlunck G, Hansen LL, Feltgen N, Martin G, Agostini HT, Pielen A. Increased expression of angiogenic and inflammatory proteins in the vitreous of patients with ischemic central retinal vein occlusion. PLoS One 2015; 10:e0126859[PMID: 25978399].

52. Hu A, Schmidt MHH, Heinig N. Microglia in retinal angiogenesis and diabetic retinopathy. Angiogenesis 2024; 27:311-31. [PMID: 38564108].

53. Al-Shabrawey M, Elsherbiny M, Nussbaum J, Othman A, Megyerdi S, Tawfik A. Targeting Neovascularization in Ischemic Retinopathy: Recent Advances. Expert Rev Ophthalmol 2013; 8:267-86. [PMID: 25598837].

54. Campochiaro PA. Molecular pathogenesis of retinal and choroidal vascular diseases. Prog Retin Eye Res 2015; 49:67-81. [PMID: 26113211].

55. Ramakrishnan S, Anand V, Roy S. Vascular endothelial growth factor signaling in hypoxia and inflammation. J Neuroimmune Pharmacol 2014; 9:142-60. [PMID: 24610033].

56. Gui F, You Z, Fu S, Wu H, Zhang Y. Endothelial Dysfunction in Diabetic Retinopathy. Front Endocrinol (Lausanne) 2020; 11:591-[PMID: 33013692].

57. Goel S, Duda DG, Xu L, Munn LL, Boucher Y, Fukumura D, Jain RK. Normalization of the vasculature for treatment of cancer and other diseases. Physiol Rev 2011; 91:1071-121. [PMID: 21742796].

58. Qian C, Liu C, Liu W, Zhou R, Zhao L. Targeting vascular normalization: a promising strategy to improve immune-vascular crosstalk in cancer immunotherapy. Front Immunol 2023; 14:1291530[PMID: 38193080].

59. Go S, Lim RR, Chaurasia SS. S100A9 plays a proinflammatory role in the progression of diabetic retinopathy. [abstract]. Invest Ophthalmol Vis Sci 2023; 64:2046. Presented at the 2023 ARVO Annual Meeting, New Orleans, LA, April 23-27, 2023.

60. Chen B, Miller AL, Rebelatto M, Brewah Y, Rowe DC, Clarke L, Czapiga M, Rosenthal K, Imamichi T, Chen Y, Chang CS, Chowdhury PS, Naiman B, Wang Y, Yang D, Humbles AA, Herbst R, Sims GP. S100A9 induced inflammatory responses are mediated by distinct damage associated molecular patterns (DAMP) receptors in vitro and in vivo. PLoS One 2015; 10:e0115828[PMID: 25706559].

61. Schiopu A, Cotoi OS. S100A8 and S100A9: DAMPs at the crossroads between innate immunity, traditional risk factors, and cardiovascular disease. Mediators Inflamm 2013; 2013:828354[PMID: 24453429].

62. Cehofski LJ, Honoré B, Vorum H. A Review: Proteomics in Retinal Artery Occlusion, Retinal Vein Occlusion, Diabetic Retinopathy and Acquired Macular Disorders. Int J Mol Sci 2017; 18:907-[PMID: 28452939].

63. Stepanov A, Usharova SA, Malsagova KA, Moshetova LK, Turkina KI, Kopylov AT, Kaysheva AL. Tear Proteome Revealed Association of S100A Family Proteins and Mesothelin with Thrombosis in Elderly Patients with Retinal Vein Occlusion. Int J Mol Sci 2022; 23:14653-[PMID: 36498980].

64. Rosenfeld PJ, Heier JS, Hantsbarger G, Shams N. Tolerability and efficacy of multiple escalating doses of ranibizumab (Lucentis) for neovascular age-related macular degeneration. Ophthalmology 2006; 113:623.e1[PMID: 16581423].

65. Subhi Y, Schneider M, Hajari JN, la Cour M. Injection burden and treatment intervals of aflibercept in observe-and-plan regimen for neovascular age-related macular degeneration. Acta Ophthalmol 2024; 102:821-7. [PMID: 38733136].

66. Fauser S, Schroeder S, Caramoy A, Kirchhof B, Lappas A. Intraocular inflammation after intravitreal ranibizumab injections. Acta Ophthalmol 2011; 89:e98-9. [PMID: 20384590].

67. Matsumoto H, Hoshino J, Numaga S, Mimura K, Asatori Y, Akiyama H. Retinal vasculitis after intravitreal aflibercept 8 mg for neovascular age-related macular degeneration. Jpn J Ophthalmol 2024; 68:531-7. [PMID: 39162906].

68. Chandra S, Sheth J, Anantharaman G, Gopalakrishnan M. Ranibizumab-induced retinal reperfusion and regression of neovascularization in diabetic retinopathy: An angiographic illustration. Am J Ophthalmol Case Rep 2018; 9:41-4. [PMID: 29468217].

69. Kim YJ, Yeo JH, Son G, Kang H, Sung YS, Lee JY, Kim JG, Yoon YH. Efficacy of intravitreal AFlibercept injection For Improvement of retinal Nonperfusion In diabeTic retinopathY (AFFINITY study). BMJ Open Diabetes Res Care 2020; 8:e001616[PMID: 33077475].

70. Reddy RK, Pieramici DJ, Gune S, Ghanekar A, Lu N, Quezada-Ruiz C, Baumal CR. Efficacy of Ranibizumab in Eyes with Diabetic Macular Edema and Macular Nonperfusion in RIDE and RISE. Ophthalmology 2018; 125:1568-74. [PMID: 29752001].

71. Toto L, D'Aloisio R, Libertini D, D'Onofrio G, De Nicola C, Mastropasqua R, Chiarelli AM. Study of Nonperfusion Area Changes after Ranibizumab Intravitreal Injection for Diabetic Macular Edema by Means of Widefield OCT Angiography. Ophthalmic Res 2023; 66:8-13. [PMID: 35313317].

72. Suzuma K, Takagi H, Otani A, Oh H, Honda Y. Expression of thrombospondin-1 in ischemia-induced retinal neovascularization. Am J Pathol 1999; 154:343-54. [PMID: 10027393].

Articles are provided courtesy of Emory University and The Abraham J. & Phyllis Katz Foundation. The print version of this article was created on 5 August 2026. This reflects all typographical corrections and errata to the article through that date. Details of any changes may be found in the online version of the article.